Supporting Information

Efficient Electrocatalytic Proton Reduction with Carbon Nanotube-Supported Metal-Organic Frameworks

Daniel Micheroni, Guangxu Lan, and Wenbin Lin*

Department of Chemistry, The University of Chicago, Chicago, IL 60637, United States

Correspond author Email: wenbinlin@uchicago.edu

Contents:

Materials: All reagents and solvents were purchased from commercial sources and used without further purification unless otherwise stated: methyl-4-formylbenzoat; dichloromethane, 2,3-dichloro-5,6,-dicyno-1,4-benzoquinone (DDQ), triethylammine (TEA); triflouroacetic acid (TFA), ethanol; sodium hydroxide; hydrochloric acid (HCl); hafnium chloride ($HfCl_4$); acetic acid; dimethylformamide (DMF). CNTs functionalized with carboxylic acid groups were purchased from Chengdu Organic Chemistry Institute (China) while unfunctionalized CNTs were purchased from Aldrich.

Synthesis of 5,15-di(p-methyl-benzoato)porphyrin (Me_2DBP)[1]

Methyl-4-formylbenzoate (520 mg, 3.16 mmol) and dipyrromethane (463 mg, 3.16 mmol) were added to a round bottom flask. To the flask 500 mL of anhydrous dichloromethane was added and degassed for 30 minutes. Trifluoroacetifc acid (0.5 mL, 6.47 mmmol) was added dropwise via a syringe. The mixture was stirred at room temperature in the dark for four hours. To the reaction mixture, 2,3-dichloro-5,6-dicyano-1,4benzoquinone (DDQ, 1085 mg, 4.74 mmol) was added and allowed to stir for an additional hour. The reaction was quenched with triethylammine (TEA, 8 mL, 57.3 mmol). The solvent was removed with a rotary evaporator and the resulting solid was purified on a silica column using a chloroform:ethyl acetate (9:1) eluent to give a deep purple solid as the product. Yield: 290 mg, 0.50 mmol (31.6%). ^{1}H-NMR (500MHz, chloroform-D, ppm): δ =10.37 (s, 2H), 9.47 (d, 4H), 9.10 (d, 4H), 8.49 (d, 4H), 8.36(d, 4H), 4.15 (s, 6H), -3.12 (s, 2H).

Synthesis of 5, 15-di(*p*-benzoato)porphyrin (H_2DBP)[1]

Me_2DBP (290 mg, 0.50 mmol) was dissolved in a mixture of 1:1 ethanol and 6M aqueous NaOH. The solution was heated to reflux under nitrogen overnight. The solution was then cooled to room temperature and then acidified to pH = 2 with 2M hydrochloric acid. The solid was collected and washed via centrifugation three times with water and dried overnight under vacuum to afford the maroon product. Yield: 257 mg, 46.5 mmol (93% yield). ^{1}H-NMR (500MHz, dimethyl sulfoxide-D_6, ppm): δ =13.33 (s, 2H), 10.69 (s, 2H), 9.69 (d, 4H), 9.06 (d, 4H), 8.43 (m, 8H), -3.35 (s, 2H).

Synthesis Hf_{12}-CoDBP

H_2DBP (1.5 mg, 2.7 μmol), hafnium(IV) chloride (1.00 mg, 3.15 μmol), and acetic acid (70 μL, 1224 umol) were combined in 1.0 mL of dimethylformamide and heated at 85 °C oven for three days. A dark red powder was collected by centrifugation and washed with DMF three times. The MOF was then metalated with 4.05 μmol of $CoCl_2 \cdot 6H_2O$ in 1 mL of DMF at 80 °C for 24 hours. The product was washed with DMF then ethanol twice and collected via centrifugation and stored in 0.5 mL of ethanol. Yield: 1.5 mg, mg (71.5%).

Alternatively, Hf_{12}-CoDBP was prepared by heating a mixture of H_2CoDBP (1.66 mg, 2.7 μmol), hafnium(IV) chloride (1.00 mg, 3.15 μmol), water (10 μL μmol), and acetic acid (70 μL, 1224 umol) in DMF at 85 °C for three days. Yield: 1.0 mg (47.7%).

Synthesis of Hf_{12}-CoDBP/CNT

H_2CoDBP (1.66 mg, 2.7 μmol), hafnium(IV) chloride (1.00 mg, 3.15 μmol), 5 mg of carboxylated multi-walled carbon nanotubes, 10 μLH_2O, and acetic acid (70 μL, 1224 umol) were combined in 1.0 mL of dimethylformamide and heated at 85 °C oven for three days. A black powder was collected by centrifugation and washed with DMF three times, ethanol twice, then stored in 0.5 mL of ethanol.

Electrochemical Methods

All electrochemical experiments were performed using a Pine Instruments WaveDriver potentiostat (Model AFP2). Non-catalytic experiments were performed with 0.1 M $TBAPF_6$ serving as the electrolyte in acetonitrile that was degassed with nitrogen for at least thirty minutes. Electrochemical experiments in aqueous solutions were performed at pH = 1 with perchloric acid; the solution was degassed with nitrogen for at least thirty minutes. If the pH was increased, the electrolyte concentration was maintained at 0.1 ClO_4^- using potassium perchlorate. Cyclic voltammetry (CV) measurements were performed in a standard three-electrode cell with a glassy carbon electrode (0.4 cm diameter) serving as the working electrode, silver/silver chloride electrode serving as the reference electrode (Calculated at 0.223 V vs the NHE from the $Fe(CN)_6$ redox couple), and a platinum counter electrode. Scan rates were 100 mV s^{-1} unless stated otherwise and all experiments were collected underneath a nitrogen atmosphere. Controlled potential electrolysis was performed in the same setup as the CV except that the electrode was

spun at 400 RPM using the RDE assembly coupled with a stir bar at 400 RPM to prevent bubbles from building up on the working electrode surface.

GC Quantification

All gas chromatography (GC) measurements were obtained using an Agilent 7890B GC system. 300 μL of headspace gas of the reaction vessel (measured to be 177 mL) was injected post controlled potential electrolysis.

XPS Characterization

X-ray photoelectron spectroscopy (XPS) data was collected using an AXIS Nova spectrometer (Kratos Analytical) with monochromatic Al Kα Xray source. For this instrument, the Al anode was powered at 10 mA and 15kV. Instrument base pressure was ca. 1×10^{-9} Torr, and the analysis area size was 0.3 × 0.7 mm^2. For calibration purposes, the binding energies were referenced to the C 1s peak at 284.8 eV. Survey spectra were collected with a step size of 1 eV and a pass energy of 160 eV, while the cobalt region was collected with a step size of 0.1 eV.

ICP-MS Characterization

ICP-MS data was obtained with an Agilent 7700x ICP-MS and analyzed using ICP-MS MassHunter version B01.03. Samples were diluted in a 2% HNO_3 matrix and analyzed with a ^{159}Tb internal standard against a 12-point standard curve over the range from 0.1 ppb to 500 ppb. The correlation was >0.9997 for all analyses of interest. Data collection was performed in spectrum Mode with five replicates per sample and 100 sweeps per replicate.

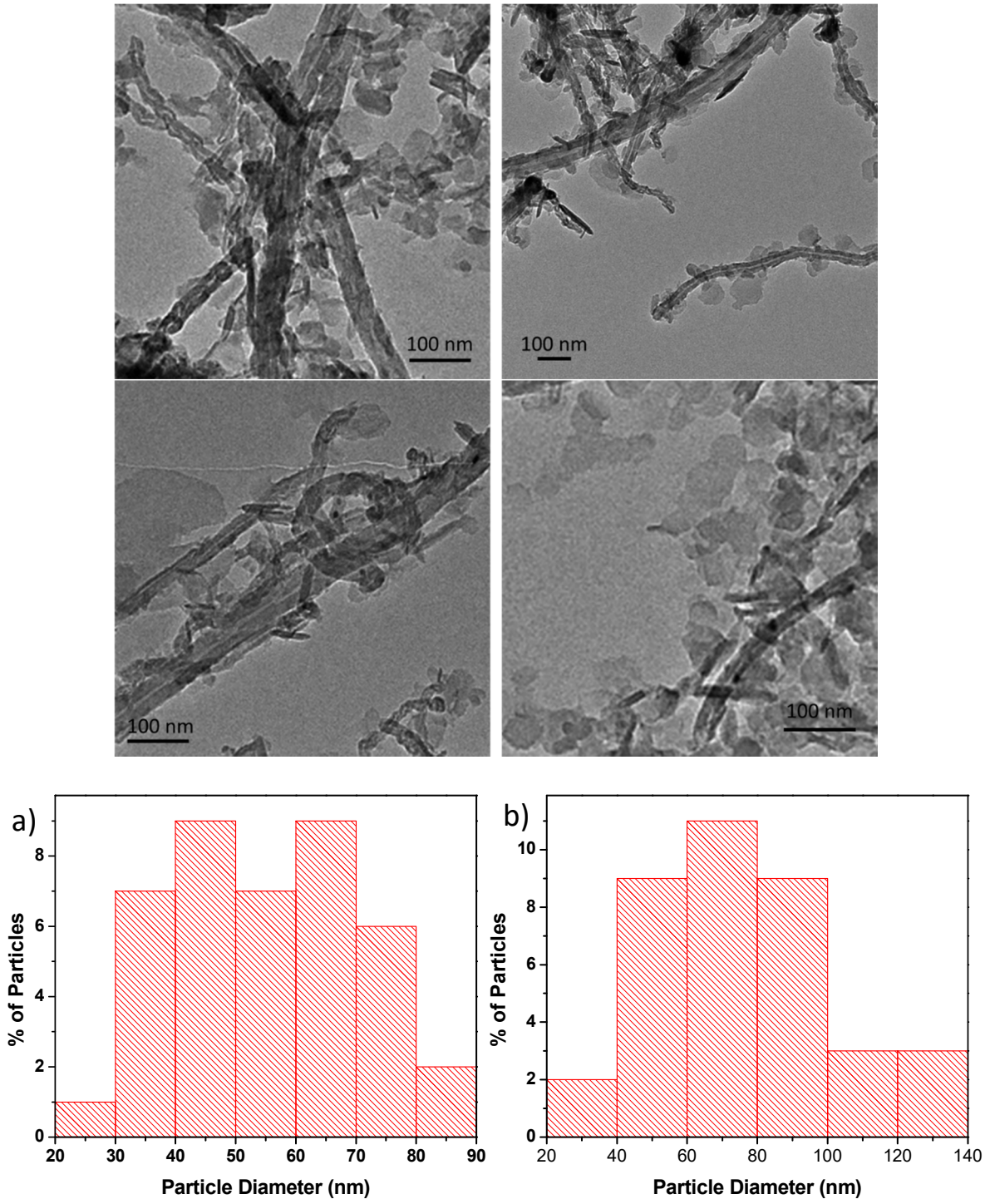

Figure S1. Histogram of the Hf_{12}-CoDBP particle sizes from distinct samples, both (a with and (b without CNT functionalization as determined by TEM above and in the primary manuscript.

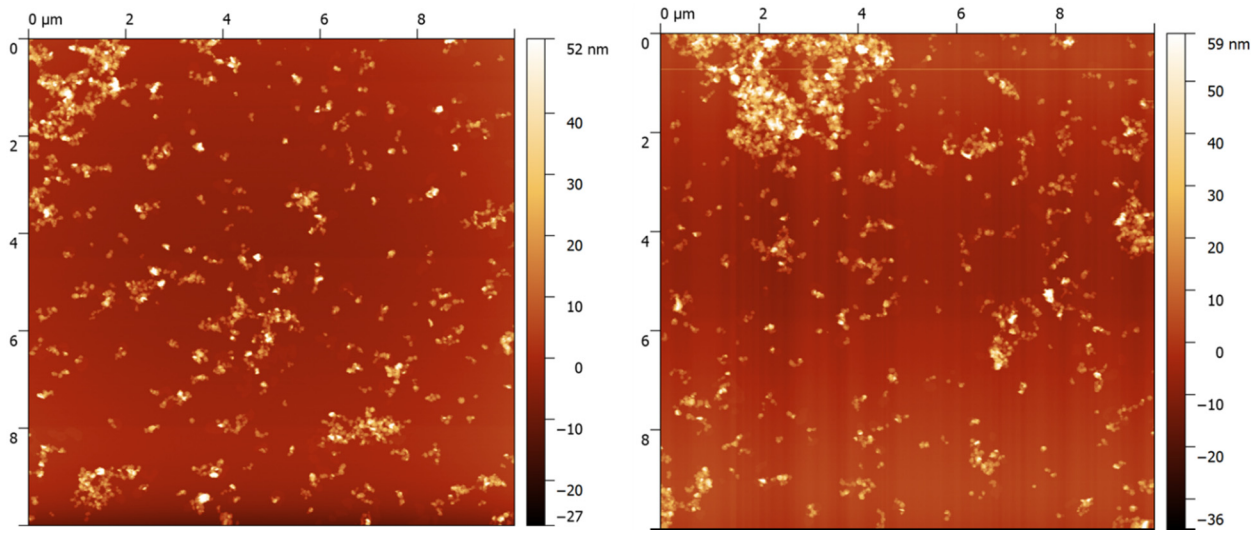

Figure S2. AFM images of two different Hf_{12}-DBP samples show consistent shape and thickness ranging from 15 to 40 nm.

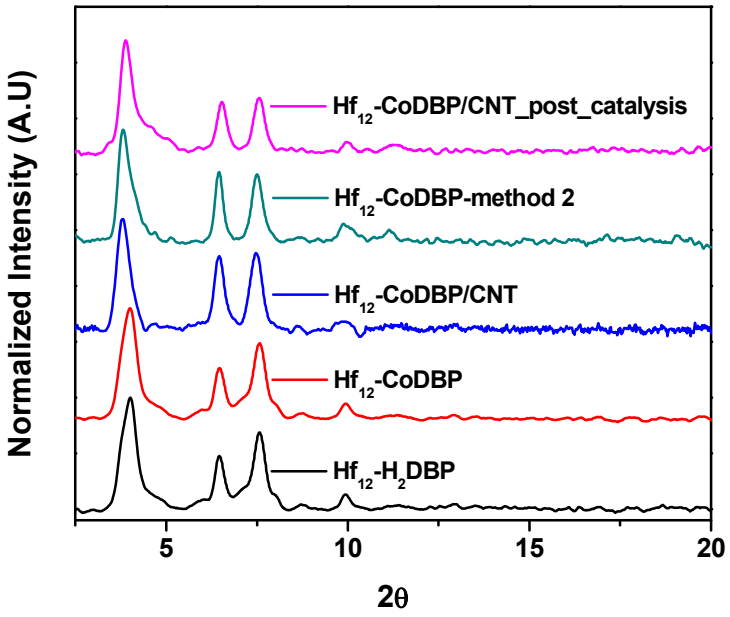

Figure S3. PXRD of Hf_{12}-CoDBP/CNT (blue) showed identical peaks to Hf_{12}-CoDBP (red and teal), and Hf_{12}-H_2DBP (black), indicating the Hf_{12}-CoDBP grown on CNT had the same crystalline structure as the parent Hf_{12}-CoDBP.

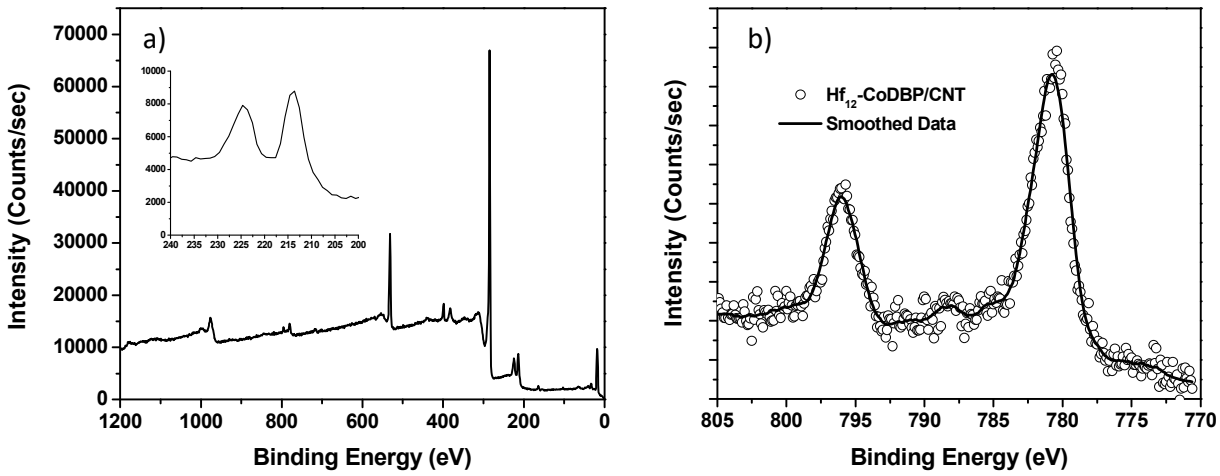

Figure S4. a) The XPS spectrum of Hf_{12}-CoDBP/CNT was used to determine the Hf to Co ratio, with the inset graph showing the $Hf4d_{3/2}$ peak. b) The cobalt region of the XPS spectrum shows Co^{III} oxidation state for Hf_{12}-CoDBP/CNT. For XPS integration, relative sensitive factors (RSFs) of 33.12 and 66.88 were used for $Co2p_{3/2}$ and $Hf4d_{3/2}$ peaks, respectively.

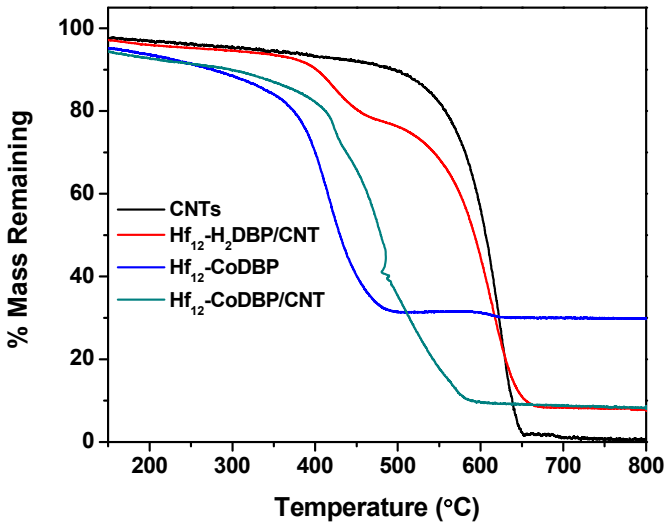

Figure S5. Comparison of TGA curves of Hf_{12}-CoDBP/CNT, CNT, and Hf_{12}-CoDBP shows that Hf_{12}-CoDBP/CNT contains ~20 wt% Hf_{12}-CoDBP with a Hf to H_2DBP ligand ratio of 1.66:1 and a Hf to CoDBP ratio of 1.46:1.

The first weight at 385 to 470 °C (13.4 %) was assigned to the degradation of the porphyrin moiety into CO_2 and metal oxides. The second weight loss at 485 to 670 °C corresponds to the decomposition of the CNTs. The weight remaining (8.25%) at > 670 °C is attributed to HfO_2. The

Hf to ligand ratio was determined from the percent weight loss of porphyrin compared to the percent HfO_2 remaining.

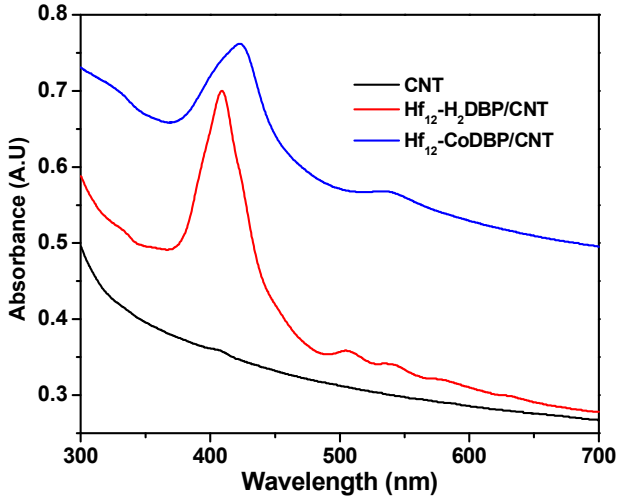

Figure S6. UV-Vis spectra of CNTs, Hf_{12}-H_2DBP/CNT and Hf_{12}-CoDBP/CNT in DMF.

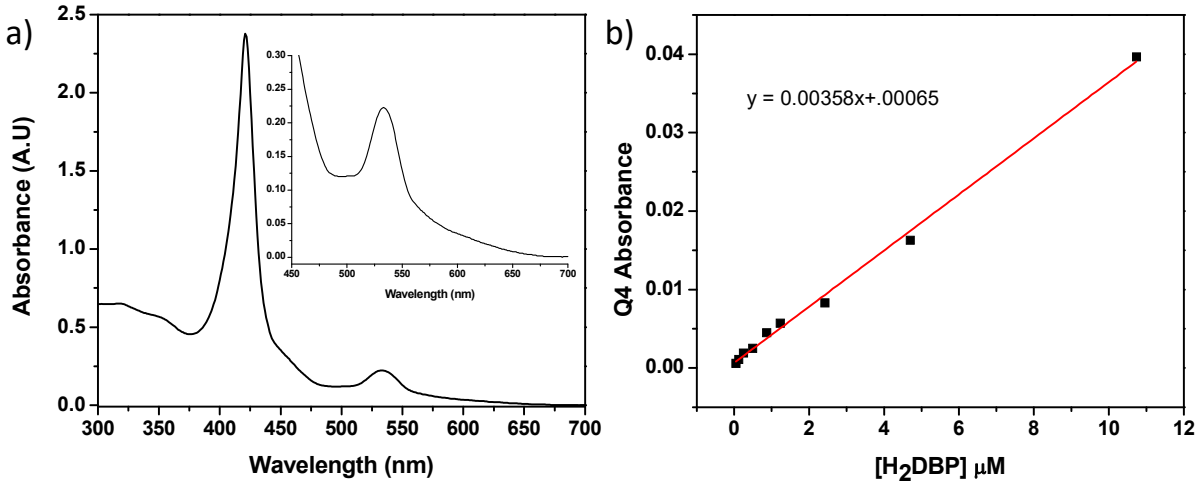

Figure S7. (a) UV-Vis spectrum of 40 μM CoDBP taken from the Hf_{12}-CoDBP growth solution. (b) The standard curve of the Q4 band for H_2DBP showing a detection limit of <1 μM. However, a slight shoulder in the CoDBP spectrum near the Q4 band makes it difficult to discern any H_2DBP species of less than 10% CoDBP. The lack of discernible Q4 band of H_2DBP in the 40 μM CoDBP taken from the Hf_{12}-CoDBP growth solution thus shows the less than 10% leaching of Co ions.

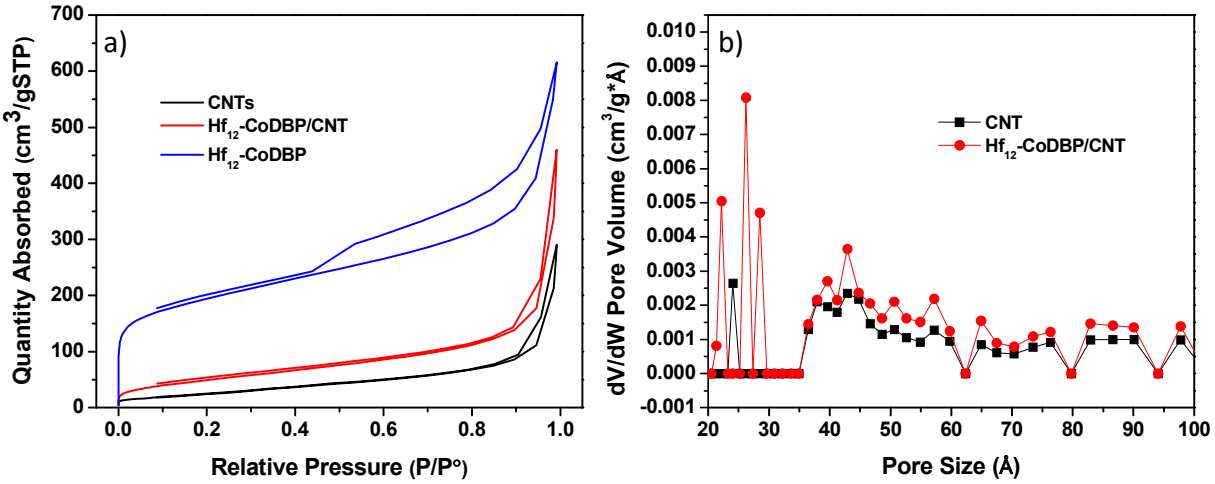

Figure S8. a) Nitrogen sorption isotherms for CNTs, Hf_{12}-CoDBP, and Hf_{12}-CoDBP/CNT afforded BET surface areas of 78.12 m^2/g, 509.3 m^2/g, and 115.14 m^2/g, respectively. b) Pore size distribution of Hf_{12}-CoDBP/CNT and CNTs as determined by the DFT method.

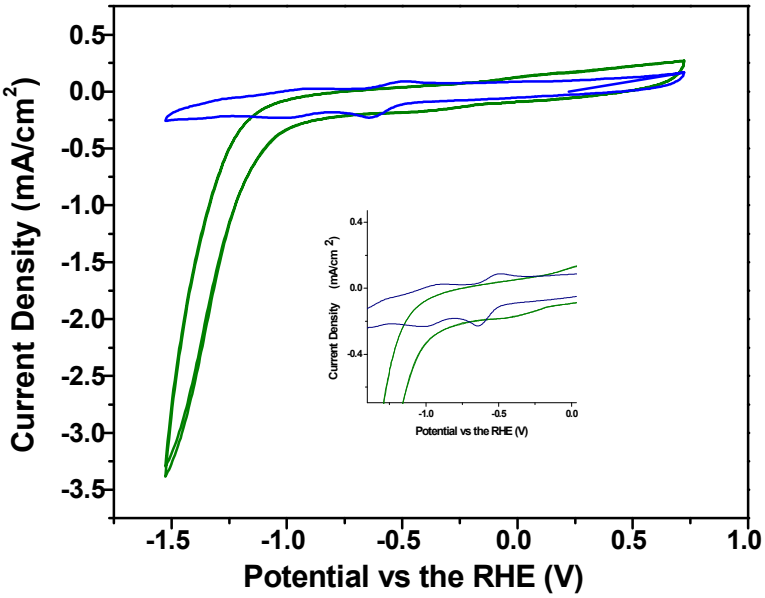

Figure S9. Cyclic voltammetry curves of Hf_{12}-CoDBP/CNT in the presence of 0.026 M TFA in acetonitrile show proton reduction consistent with a Co^{I}-H intermediate, vastly outperforming a bare glassy carbon electrode.

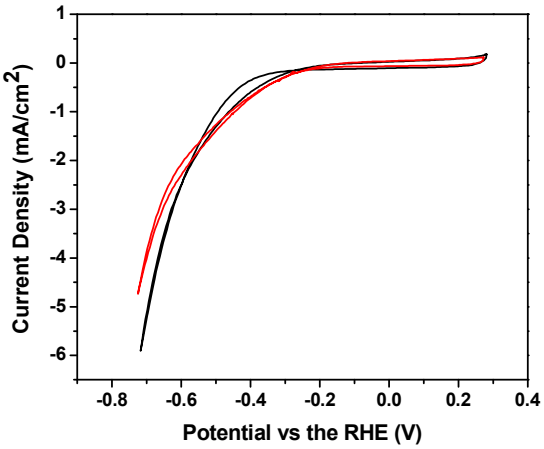

Figure S10. CV traces of Hf_{12}-CoDBP/CNT/Nafion taken with a GCE counter electrode before (red) and after bulk electrolysis (black) in pH 1 perchloric acid.

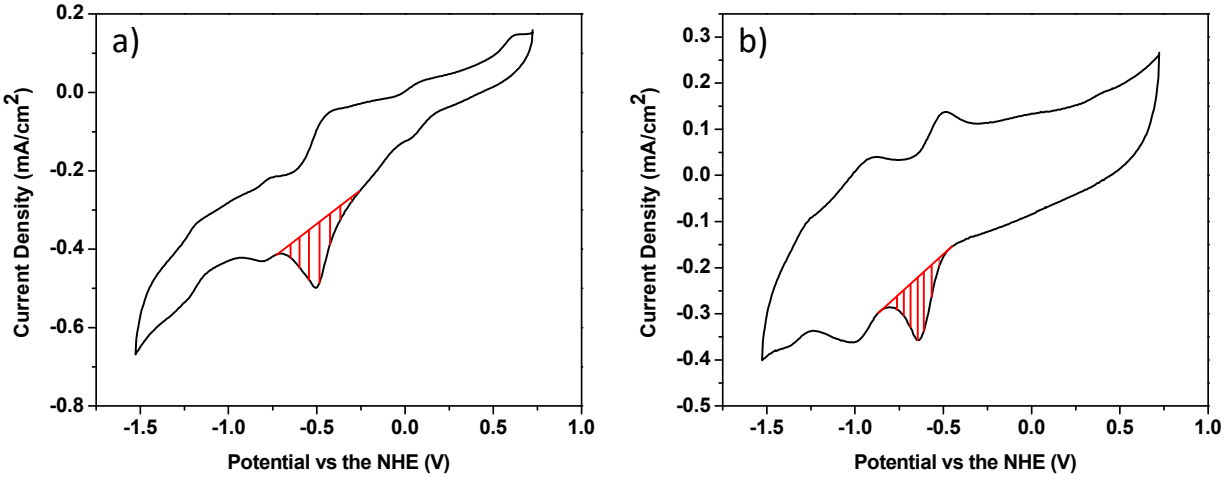

Figure S11. a) Comparison of the integrations of the first reductive peaks for Hf_{12}-CoDBP and b) Hf_{12}-CoDBP/CNT shows a 114-fold increase in the percent active sites for the Hf_{12}-CoDBP/CNT material. For a), 0.28% of the 26.1 nmol of Co centers were reduced, while for b), 31.9% of the available 1.58 nmol Co centers were reduced.

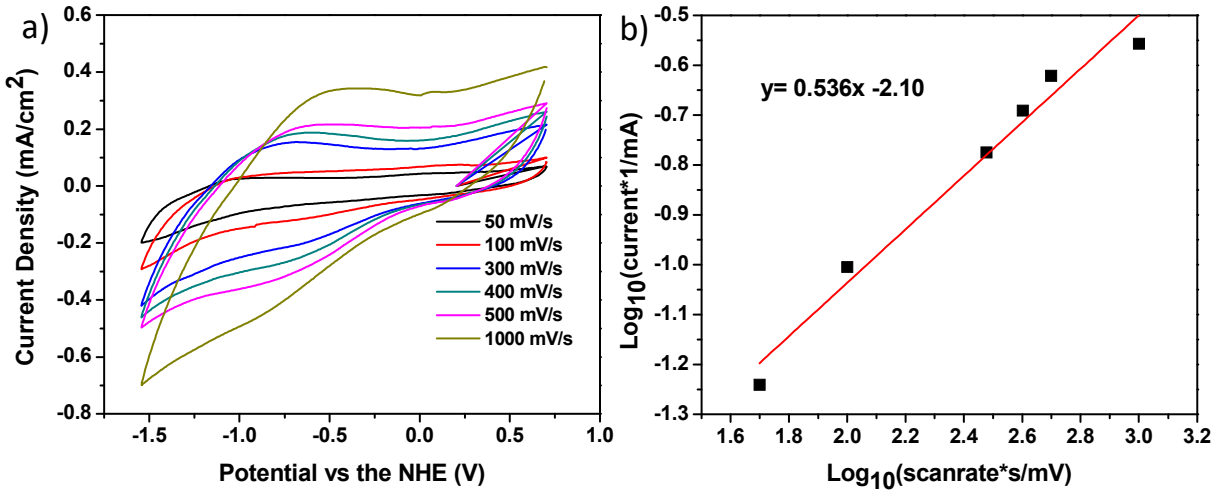

Figure S12. a) CV curves of Hf_{12}-CoDBP/CNT in ACN at varying scan rates. b) A linear relationship between $\log_{10}$(current in mA) and $\log_{10}$(scan rate in mV/s) with a slope of 0.54 suggests electron transfer occurs via charge hopping to the cobalt center.

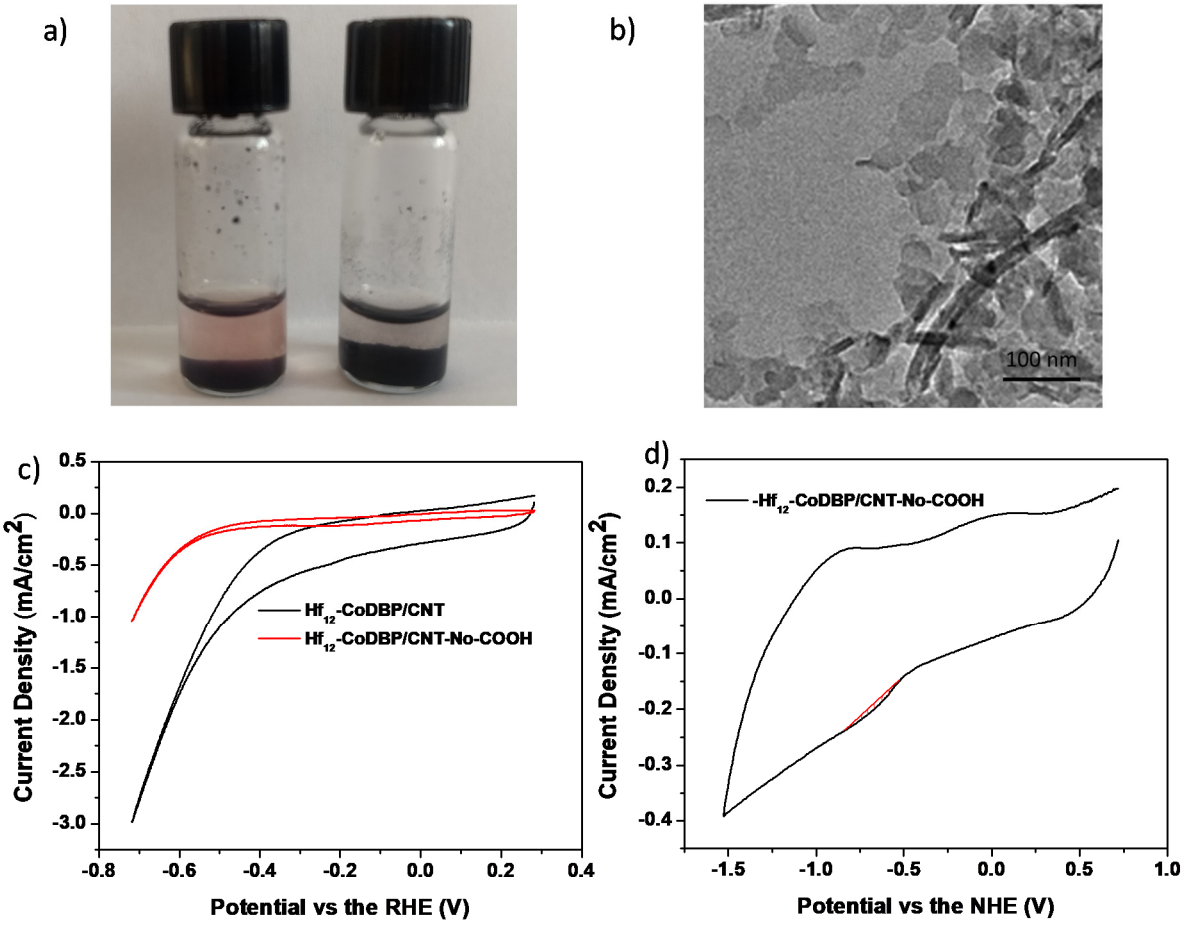

Figure S13. a) Hf_{12}-CoDBP/non-carboxylated CNT (left) but not Hf_{12}-CoDBP/CNT (right) showed the color of unbound Hf_{12}-CoDBP in the supernatant. b) TEM image of Hf_{12}-CoDBP/non-

carboxylated CNT. c) CV curve of Hf_{12}-CoDBP/CNT and Hf_{12}-CoDBP/non-carboxylated CNT at pH = 1 ($HClO_4$). d) CV curve of Hf_{12}-CoDBP/non-carboxylated CNT in 0.1 M $TBAPF_6$ dissolved in ACN shows that 0.29% of 1.81 nmol total Co on the electrode is electrochemically active.

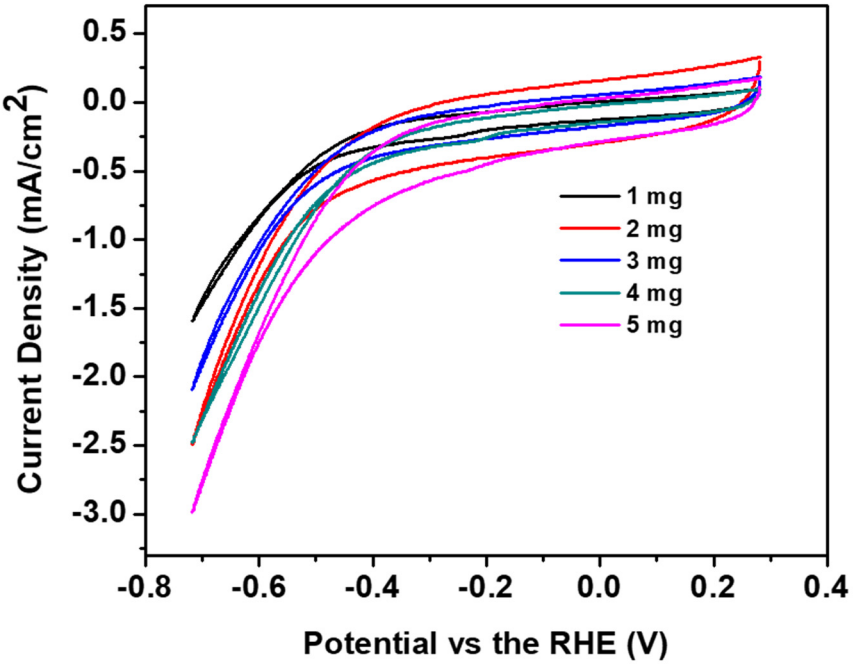

Figure S14. CV traces of 0.05 mg of Hf_{12}-CoDBP/CNT/Nafion synthesized with 1 to 5 mg of CNTs and 1.7 mg of CoDBP in pH 1 perchloric acid solutions. Increasing currents due to increasing amounts of CNT indicate the important role of carboxylated CNT in electrocatalytic activity.

Table S1: The results of 30 minutes of controlled potential electrolysis at η = 715 mV for various samples of Hf_{12}-CoDBP/CNT/Nafion with variable CNT loading in pH 1 perchloric acid.

Sample	η (mV)	μMOL H_2 Produced	TON	%Faradaic Efficiency
Hf_{12}-CoDBP/1mg-CNT	715	3.81	8.20×10^2	64.8
Hf_{12}-CoDBP/2mg-CNT	715	4.44	1.51×10^3	65.7
Hf_{12}-CoDBP/3mg-CNT	715	4.66	2.82×10^3	70.3
Hf_{12}-CoDBP/4mg-CNT	715	6.29	1.06×10^4	85.3
Hf_{12}-CoDBP/5mg-CNT	715	5.94	3.80×10^3	80.0

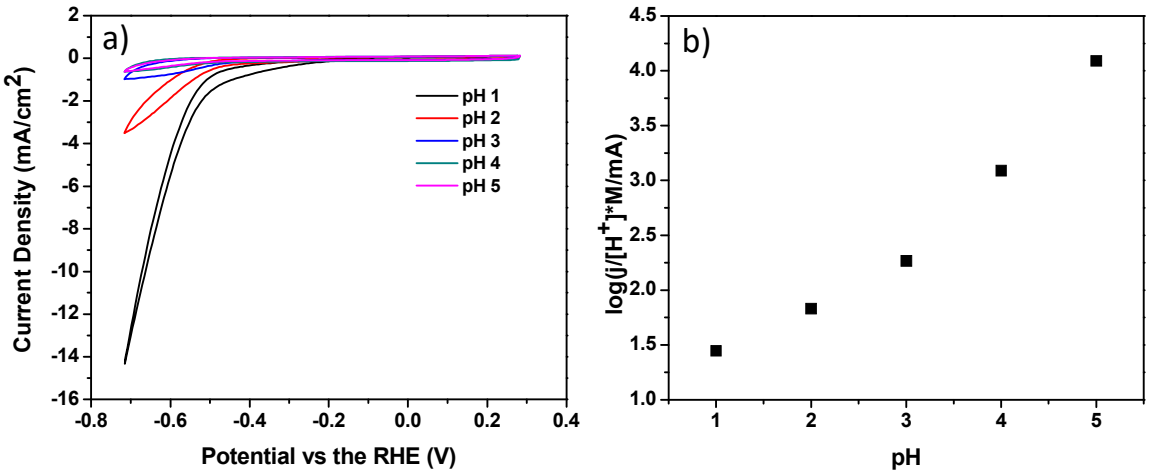

Figure S15. a) CV traces of Hf_{12}-CoDBP/CNT at varying pHs and b) the recorded current at η = 715 mV divided by proton concentration shows enhanced activity at higher pH values, indicating non-first order kinetics.

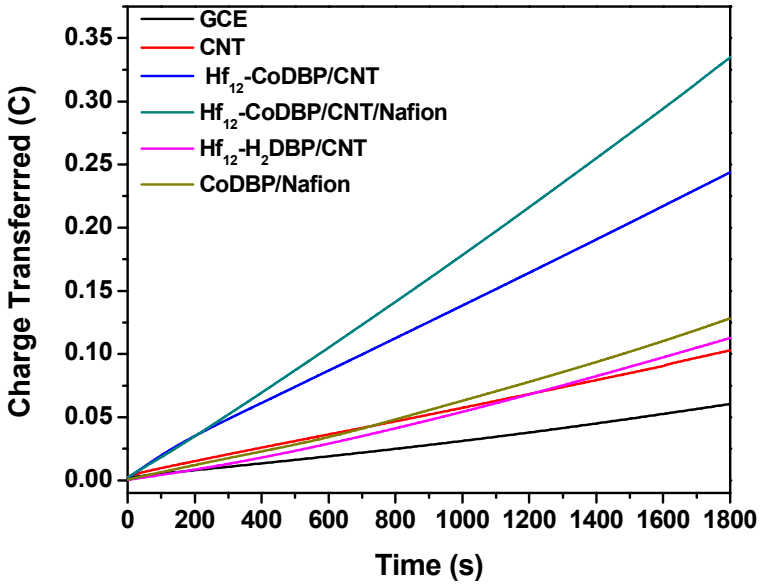

Figure S16. Controlled potential electrolysis of Hf_{12}-CoDBP/CNT and Hf_{12}-CoDBP/CNT/Nafion outperform their controls at a η of 515 mV vs the RHE at pH = 1 (perchloric acid).

Table S2: The results of controlled potential electrolysis at varying potentials show the functionalized Hf_{12}-CoDBP materials outperform the controls in both activity and Faradaic efficiency.

Sample	**η (mV)**	**μMOL H_2 Produced**	**%Faradaic Efficiency**
GCE	515	0.084	38.7
CNT	515	0.0593	14.1
CoDBP/Nafion	55	0.421	81.7
Hf_{12}-CoDBP/CNT	515	0.878	71.1
Hf_{12}-CoDBP/CNT/Nafion	515	1.41	82.9
Hf_{12}-H_2DBP/CNT	515	0.154	3.0
GCE	715	1.13	45.8
CNT	715	1.88	12.9
CoDBP/Nafion	715	1.59	43.1
Hf_{12}-CoDBP/CNT	715	10.33	93.2
Hf_{12}-CoDBP/CNT/Nafion	715	16.39	83.5
Hf_{12}-H_2DBP/CNT	715	3.39	36.8

Table S3: The efficiency of porphyrin and cobalt-containing electrocatalysts for HER.

Sample	Solvent	Ref. Electrode	H^+ Source	Potential (V)	TON	% F.E
FeTPP[2]	DMF	SCE	TEA-H^+	-1.60	22	> 95
CoPc[3]	H_3PO_4, pH 1	AgCl	H^+	-0.9	20000	N/A
CoTMAP[4]	H_2O	SCE	0.1 M TFA	-0.95	N/A	> 90
CoTPPS[5]	2M Kpi (*aq*)	SHE	H_2O, pH 7	-1.29	725	> 95
CoP[6]	PO_4^{3-}, pH 7	SCE	Benzoic acid	-1.30	n/a	n/a
Co($dmgBF_2$)$_2$[7]	ACN	SCE	HCl	-0.37 V	11	90
Cobalt Tetraazamacrocycle[8]	$NaClO_4$ (*aq*)	SCE	H^+, pH 2.2	-0.93	22	81
CoPY5Me$_2$[9]	PO_4^{3-}, pH 7	SHE	H_2O	-1.30	55000	100
CoPY4[10]	H_2O/ACN	SCE	TFA	N/A	40	N/A
Co(mnt)$^-_2$[11]	H_2O/ACN	SCE	Ascorbic acid, pH 4	-1.37	3450	N/A
CoMP11-AC[12]	H_2O	Ag/AgCl	H_2O	-1.5	25000	> 95

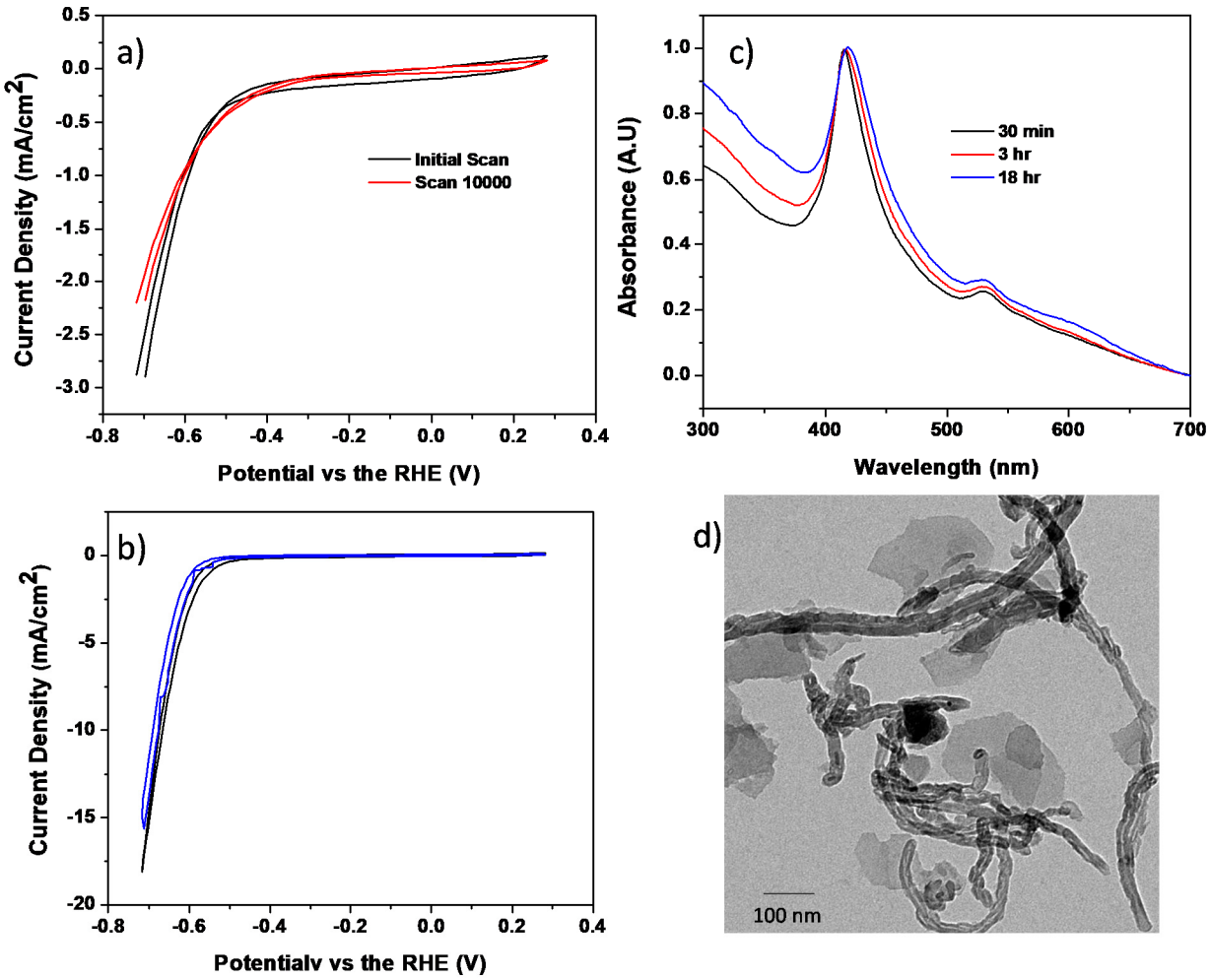

Figure S17. a) Hf_{12}-CoDBP/CNT/Nafion shows consistent CV curves after 10,000 CV scans and b) after 30 minutes of controlled potential electrolysis at 715 mV vs the RHE in pH = 1 $HClO_4$. c) Hf_{12}-CoDBP/CNT/Nafion shows no change in its UV-Visible spectra after bulk electrolysis at η = 615 mV for various time lengths, d) Hf_{12}-CoDBP/CNT/Nafion shows no Co nanoparticle formation in the TEM after electrolysis at an overpotential of 715 mV for one hour.

References:

(1) Lu, K.; He, C.; Lin, W., Nanoscale Metal-Organic Framework for Highly Effective Photodynamic Therapy of Resistant Head and Neck Cancer. *J. Am. Chem. Soc.* **2014,** *136* (48), 16712-16715.

(2) Bhugun, I.; Lexa, D.; Saveant, J.-M., Homogeneous Catalysis of Electrochemical Hydrogen Evolution by Iron(0) Porphyrins. *J. Am. Chem. Soc.* **1996,** *118* (16), 3982-3.

(3) Zhao, F.; Zhang, J.; Abe, T.; Wohrle, D.; Kaneko, M., Electrocatalytic proton reduction by phthalocyanine cobalt derivatives incorporated in poly(4-vinylpyridine-co-styrene) film. *J. Mol. Catal. A Chem.* **1999,** *145* (1-2), 245-256.

(4) Kellett, R. M.; Spiro, T. G., Cobalt(I) porphyrin catalysts of hydrogen production from water. *Inorg. Chem.* **1985,** *24* (15), 2373-7.

(5) Beyene, B. B.; Mane, S. B.; Hung, C.-H., Highly efficient electrocatalytic hydrogen evolution from neutral aqueous solution by a water-soluble anionic cobalt(II) porphyrin. *Chem. Commun. (Cambridge, U. K.)* **2015,** *51* (81), 15067-15070.

(6) Natali, M.; Luisa, A.; Iengo, E.; Scandola, F., Efficient photocatalytic hydrogen generation from water by a cationic cobalt(ii) porphyrin. *Chem. Commun. (Cambridge, U. K.)* **2014,** *50* (15), 1842-1844.

(7) Hu, X.; Cossairt, B. M.; Brunschwig, B. S.; Lewis, N. S.; Peters, J. C., Electrocatalytic hydrogen evolution by cobalt difluoroboryl-diglyoximate complexes. *Chem. Commun. (Cambridge, U. K.)* **2005,** (37), 4723-4725.

(8) McCrory, C. C. L.; Uyeda, C.; Peters, J. C., Electrocatalytic Hydrogen Evolution in Acidic Water with Molecular Cobalt Tetraazamacrocycles. *J. Am. Chem. Soc.* **2012,** *134* (6), 3164-3170.

(9) Sun, Y.; Bigi, J. P.; Piro, N. A.; Tang, M. L.; Long, J. R.; Chang, C. J., Molecular Cobalt Pentapyridine Catalysts for Generating Hydrogen from Water. *J. Am. Chem. Soc.* **2011,** *133* (24), 9212-9215.

(10) Bigi, J. P.; Hanna, T. E.; Harman, W. H.; Chang, A.; Chang, C. J., Electrocatalytic reduction of protons to hydrogen by a water-compatible cobalt polypyridyl platform. *Chem. Commun. (Cambridge, U. K.)* **2010,** *46* (6), 958-960.

(11) McNamara, W. R.; Han, Z.; Yin, C.-J.; Brennessel, W. W.; Holland, P. L.; Eisenberg, R., Cobalt-dithiolene complexes for the photocatalytic and electrocatalytic reduction of protons in aqueous solutions. *Proc. Natl. Acad. Sci. U. S. A.* **2012,** *109* (39), 15594-15599, S15594/1-S15594/8.

(12) Kleingardner, J. G.; Kandemir, B.; Bren, K. L., Hydrogen Evolution from Neutral Water under Aerobic Conditions Catalyzed by Cobalt Microperoxidase-11. *J. Am. Chem. Soc.* **2014,** *136* (1), 4-7.